Journal of Sound and Vibration (1999) **224**(2), 243–266
Article No. jsvi.1998.2108, available online at http://www.idealibrary.com on IDEAL®

CONCENTRATED FORCE EXCITATION OF DEEP BEAMS

IN MEMORY OF PROFESSOR MANFRED HECKL

B. A. T. PETERSSON
*Department of Aeronautical and Automotive Engineering, Loughborough University, Loughborough LE*11 3*TU, England*

(*Received* 15 *June* 1998, *and in final form* 4 *December* 1998)

The influence of the shear–tensional near field on the dynamic characteristics of force-excited deep beams is addressed. From a transform solution, approximations are derived and analysed for several configurations. The dynamic characteristics are examined in terms of the "point" mobility, established on a complex power basis. It is found that both the real and imaginary parts are significantly influenced by the shear–tensional nearfield in an intermediate region between a slender beam behaviour and an asymptotic waveguide behaviour. The influence manifests itself in an elevated real part owing to "leakage" from the evanescent field to the propagating one for real materials possessing losses and in a logarithmic weighting of the stiffness controlled imaginary part. No explicit dependence on the size of the indenter is identified. The estimation procedures developed, distinguishing between moderately deep and deep beams, are physically valid in a qualitative sense but furnish conservative estimates for the real part of the force mobility, while those for the corresponding imaginary part slightly over-estimate the antiresonant region and either give the overall trend or an approximate influence of the excitation distribution in the upper range of Helmholtz numbers for moderately deep and deep beams respectively.

1. INTRODUCTION

The implications of concentrated force and moment excitation of linearly elastic, homogeneous thick plates and deep beams were treated in reference [1]. For the force and moment-excited plate as well as the moment-excited deep beam, physically correct descriptions were derived for the shear–tensional nearfield leading to manageable closed-form expressions for structures thick or deep in comparison with the typical size of the indenter. Regarding the force mobility of arbitrarily deep beams, similar descriptions were not developed.

In a broad sense the shear–tensional nearfield problem, which relates to a variety of engineering applications ranging from ultrasonic metal forming to earthquake-safe design, has attracted substantial attention. The particular aspect of the influence of a shear–tensional nearfield in the two-dimensional case,

0022–460X/99/270243 + 24 $30.00/0

surprisingly however, is rarely found directly addressed and reported in the literature. Lamb [2] and Miller and Pursey [3] considered the two-dimensional problem in terms of an infinite strip vibrating normally to the free surface of an elastic half-space and radiating to its interior whilst no attempt was made to clarify and interpret the nearfield. Heckl [4] also considered the case of a line force on an elastic half-space and established numerically an expression for the imaginary part of the mobility. The plate, subject to a line force, was studied by Ljunggren [5] who obtained a series solution for the contributions to the imaginary part of the mobility from the poles associated with Lamb waves [6]. A comparison, however, was made with an approximation for the influence of shear–tensional nearfield developed from the field due to multiple point forces. This expression, thus based on a plate behaviour (plane strain), exhibits a logarithmic dependence on the ratio of plate thickness to width of the line indenter and results in a lower estimate of the nearfield effect than that of the series solution.

Herein the two-dimensional waveguide (plane stress) problem is revisited whereby the shear–tensional near-field is considered in particular, in an effort to supplement the previous study. Drawing upon the limited discrepancy in dynamic characteristics for different applied stress fields demonstrated in reference [1], the arbitrarily deep beam is assumed subject to force excitation via a soft indenter, establishing a uniform stress at the excitation area.

2. THEORETICAL ANALYSIS

2.1. FINITE DEPTH

One of the primary objectives in reference [1] was to investigate the significance of the nearfield due to concentrated excitation and efforts were made to establish closed form expressions for the associated effects. Assuming linearly elastic material properties and employing a continuum formulation, integral solutions for point mobilities of arbitrarily deep beams were developed on a complex power basis. Regarding the beam case the asymptotic approach adopted for the description of the nearfield effects was found valid only with respect to moment excitation and an expression for force excitation remains.

With the beam mobility from reference [1] which, normalized with respect to the real-valued characteristic mobility of a shear beam, $Y_{sh} = 1/(2\rho c_T \ell t)$, of width t and height 2ℓ, see Figure 1, is given by,

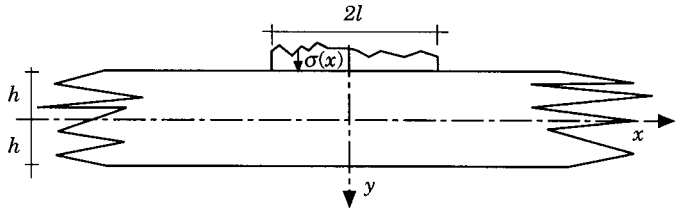

Figure 1. Force excited, deep beam.

$$\overline{Y^{C\infty}_{\nu F,s}} = -\frac{1}{2\pi}(k_T\ell)\int_{-\infty}^{\infty}\left[\frac{\sin k_T\ell\kappa}{k_T\ell\kappa}\right]\sqrt{\kappa^2-\frac{1-\nu}{2}}\left\{\frac{1}{\bar{N}_1}+\frac{1}{\bar{N}_2}\right\}\frac{e^{ik_T\ell\kappa}}{k_T\ell\kappa}\,d\kappa, \tag{1}$$

where,

$$\overline{N}_1 = (2\kappa^2-1)^2\tanh\left(k_Th\sqrt{\kappa^2-\frac{1-\nu}{2}}\right) - 4\kappa^2\sqrt{\kappa^2-\frac{1-\nu}{2}}\sqrt{\kappa^2-1}\tanh(k_Th\sqrt{\kappa^2-1}) \tag{2}$$

and

$$\overline{N}_2 = (2\kappa^2-1)^2\coth\left(k_Th\sqrt{\kappa^2-\frac{1-\nu}{2}}\right) - 4\kappa^2\sqrt{\kappa^2-\frac{1-\nu}{2}}\sqrt{\kappa^2-1}\coth(k_Th\sqrt{\kappa^2-1}), \tag{3}$$

the dynamic characteristics can be detailed for a number of structural configurations.

For small k_Th, i.e., slender beams, the hyperbolic functions can be expanded which, for the two parts of the integrand corresponding to anti-symmetric and symmetric motion respectively, means,

$$g_I \to \frac{1}{(k_Th)(k_T\ell)}\left[\frac{\sin k_T\ell\kappa}{k_T\ell\kappa}\right]\frac{e^{ik_T\ell\kappa}}{\kappa}\frac{1}{(2\kappa^2-1)^2-4\kappa^2(\kappa^2-1)},$$

$$g_{II} \to \frac{h}{\ell}\left[\frac{\sin k_T\ell\kappa}{k_T\ell\kappa}\right]\frac{e^{ik_T\ell\kappa}}{\kappa}\frac{(\kappa^2-(1-\nu)/2)}{(2\kappa^2-1)^2-4\kappa^2(\kappa^2-(1-\nu)/2)}.$$

The first part has a real-valued pole at $\kappa = 0$, for which, taking the Cauchy principal value, the contribution becomes,

$$\overline{{}_IR_0} = -i/(k_T\ell)(\ell/H). \tag{4}$$

For the second part there are three real-valued poles at $\kappa = 0$ and $\kappa = \pm\sqrt{1/2(1+\nu)}$. The contribution from the pole at zero in this case becomes,

$$\overline{{}_{II}R_0} = i[(1-\nu)/8](k_T\ell)(H/\ell), \tag{5}$$

while that of the quasi-longitudinal wave is found from a contour integration in the upper half-plane to be given by,

$$\overline{{}_{II}R_L} = i[\nu^2/8(1+\nu)](k_T\ell)(H/\ell)[1-ik_T\ell/\sqrt{2(1+\nu)}] \tag{6}$$

for small Helmholtz numbers.

Upon including also the next term in the expansions of the hyperbolic functions the first part of the integrand in equation (1) is now found to be,

$$g_I \to [1/(k_T h)(k_T \ell)][\sin k_T \ell\kappa / k_T \ell\kappa] e^{ik_T \ell\kappa}/\kappa \times \frac{1}{1 + \{4\kappa^4((1-\nu)/2 - 1) - 4\kappa^2[(1-\nu)/2] + 3\kappa^2 + (1-\nu)/2\}(k_T h)^2/3},$$

and upon retaining only the higher order terms,

$$g_I \to \frac{-3}{2(k_T h)^3 (k_T \ell)(1+\nu)} \left[\frac{\sin k_T \ell\kappa}{k_T \ell\kappa}\right] \frac{e^{ik_T \ell\kappa}}{\kappa} \frac{1}{\kappa^4 - 3/2(k_T h)^2 (1+\nu)}.$$

This expression reveals the poles associated with the flexural wave, i.e.,

$$\kappa_B = \pm \sqrt[4]{3/2(k_T h)^2 (1+\nu)}; \quad \kappa_{iB} = \pm i \sqrt[4]{3/2(k_T h)^2 (1+\nu)}.$$

Again, by means of a contour integration in the upper half-plane,

$$\overline{{}_I R_B} \to [i/2(k_T \ell)](\ell/H)[1 - ik_T \ell^4 \sqrt{3/2(k_T h)^2 (1+\nu)}], \tag{7}$$

as well as,

$$\overline{{}_I R_{iB}} \to [i/2(k_T \ell)](\ell/H)[1 - k_T \ell^4 \sqrt{3/2(k_T h)^2 (1+\nu)}]. \tag{8}$$

The second part of the integral can be found to tend to,

$$g_{II} \to -\frac{h}{\ell}\left[\frac{\sin k_T \ell\kappa}{k_T \ell\kappa}\right] \frac{e^{ik_T \ell\kappa}}{\kappa} \times \left\{\left(\kappa^2 - \frac{1-\nu}{2}\right) \Big/ \left(4\left(\frac{1+\nu}{2}\right) - \frac{(k_T h)^2}{3}\right)\right\} \Big/ \left[-\left(1 - \frac{1-\nu}{2}\frac{(k_T h)^2}{3}\right) \Big/ \left(4\left(\frac{1+\nu}{2}\right) - \frac{(k_T h)^2}{3}\right) + \kappa^2\right]$$

having poles at

$$\kappa = \pm \sqrt{\left(1 - \frac{1-\nu}{2}\frac{(k_T h)^2}{3}\right) \Big/ \left(4\left(\frac{1+\nu}{2}\right) - \frac{(k_T h)^2}{3}\right)} \to \frac{1}{\sqrt{2(1+\nu)}}.$$

for slender beams. These are thus the same quasi-longitudinal poles as found above. For deeper beams, on the other hand,

$$g_{II} \to -\frac{3}{2}\frac{h}{\ell}\left[\frac{\sin k_T \ell\kappa}{k_T \ell\kappa}\right] \frac{e^{ik_T \ell\kappa}}{\kappa} \frac{2\kappa^2 - 1 - \nu)}{(6(1+\nu) - (k_T h)^2)} \Big/ \left[\kappa^2 - \frac{1}{2}\frac{(6 - (1-\nu)(k_T h)^2)}{(6(1+\nu) - (k_T h)^2}\right],$$

$$k_T h \leqslant \sqrt{6 - \frac{7}{1+\nu} \underset{(-)}{+} \sqrt{\left(6 - \frac{7}{1+\nu}\right)^2 + 48}},$$

where the region of validity is dictated by the expansion. Following the

procedure used above leads to the result,

$$\overline{{}_{II}R_L} \to \left[\mathrm{i} + k_T l\sqrt{\frac{1}{2}\frac{(6-(1-\nu)(k_T h)^2)}{(6(1+\nu)-(k_T h)^2}}\right] \times \left(\frac{9\nu^2(H/\ell)k_T\ell}{(72(1+\nu)-3(2-\nu^2)(k_T\ell)^2(H/\ell)^2+[(1-\nu)/8](k_T\ell)^4(H/\ell)^4)}\right). \quad (9)$$

The asymptote for slender beams as the Helmholtz number, $k_T\ell$, tends to zero therefore becomes,

$$\overline{Y^{C\infty}_{\nu F,\,s}} \to \overline{{}_{I}R_0} + \overline{{}_{II}R_0} + \overline{{}_{II}R_L} + \overline{{}_{I}R_B} + \overline{{}_{I}R_{iB}},$$

or

$$\overline{Y^{C\infty}_{\nu F,\,s}} \to \frac{k_T\ell}{8(1+\nu)}\left(\frac{H}{\ell}\right)\left[\frac{k_T\ell}{\sqrt{2(1+\nu)}}+\mathrm{i}\right] + \frac{\mathrm{i}(1-\mathrm{i})}{2\sqrt{k_T\ell}}\left(\frac{6}{1+\nu}\right)^{1/4}\left(\frac{\ell}{H}\right)^{3/2}, \quad (10)$$

whereas when the beam depth is increased, equation (6a) must be employed instead of equation (6) as noted above and,

$$\overline{Y^{C\infty}_{\nu F,\,s}} \to \frac{(1-\mathrm{i})}{2\sqrt{k_T\ell}}\left(\frac{6}{1+\nu}\right)^{1/4}\left(\frac{\ell}{H}\right)^{3/2} + k_T\ell\left(\frac{H}{\ell}\right)\left\{\frac{\mathrm{i}(1-\nu}{8} + \left[\mathrm{i} + k_T\ell\sqrt{\frac{1}{2}\frac{(6-(1-\nu)(k_T h)^2)}{6(1+\nu)-(k_T h)^2)}}\right] \times (9\nu^2/(72(1+\nu)-3(2-\nu^2)(k_T\ell)^2(H/\ell)^2+[(1-\nu)/8](k_T\ell)^4(H/\ell)^4))\right\} \quad (11)$$

which, for a Poisson's ratio around 0.3, is typically valid up to the dilatational resonance.

2.2. INFINITE DEPTH

In the case where H/ℓ becomes very large and tends to infinity, the expansions employed above are no longer valid. Instead, the asymptote introduced in reference [1, see equation (6)] applies and as demonstrated in Appendix I, the transform solution for a soft indenter becomes,

$$\overline{Y^{C\infty}_{\nu F,\,s}} = -\frac{2\mathrm{i}}{\pi}k_T\ell\int_0^\infty\left[\frac{\sin k_T\ell\kappa}{k_T\ell\kappa}\right]^2\frac{\sqrt{\kappa^2-(1-\nu)/2}\,\mathrm{d}\kappa}{[(2\kappa^2-1)^2-4\kappa^2\sqrt{k^2-(1-\nu/2)}\sqrt{\kappa^2-1}]}, \quad (12)$$

where the branch points at $\kappa=\sqrt{1-\nu/2}$ and $\kappa=1$ must be observed. Additionally, there is the pole related to the Rayleigh wave, the locus of which can be obtained numerically and which for a Poisson's ratio around 0·3 is found to be approximately at $\kappa_R \approx 1{\cdot}0915$. From the integrand one can infer that for

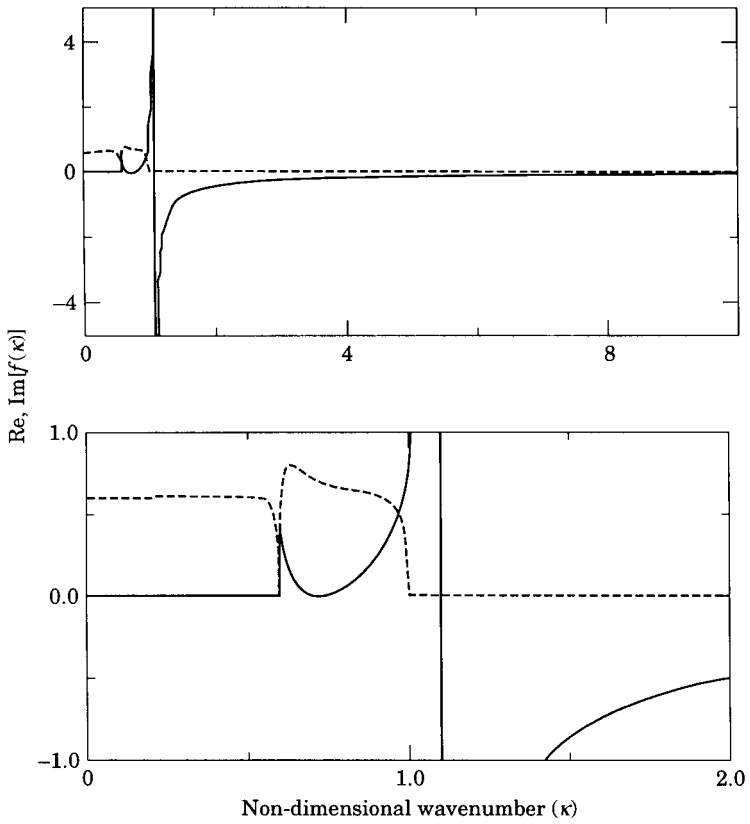

Figure 2. —, Real and ---- imaginary parts of the integrand in equation (12) for a vanishing Helmholtz number.

small Helmholtz numbers, $k_T\ell$, the integral becomes independent of this number and thus constituting simply a complex constant. Accordingly, this means that as long as the 'sinc' factor of the integrand, associated with the excitation, can be set to unity as an acceptable approximation, the slopes of the real and imaginary parts of the mobility are known.

In Figure 2 are shown the real and imaginary parts of the integrand for small Helmholtz numbers, taking the branch points into account. It is seen that a contribution to the real part of the mobility, associated with the imaginary part of the integrand, is only obtained for $\kappa \leqslant 1$ whereas the imaginary part contains contributions from the lowest branch point and upwards. The imaginary part of the integrand is further seen to be essentially constant and approximately equal to its value at the origin. This means that the real part of the mobility can be approximated by multiplying the factor in front of the integral by the value of the integrand at the origin. Thus, the real part of the mobility is approximately found from,

$$\mathrm{Re}[\overline{Y^{C\infty}_{\nu F,\,s}}] \approx \frac{2}{\pi} k_T\ell \sqrt{\frac{1-\nu}{2}} \int_0^1 \left[\frac{\sin k_T\ell\kappa}{k_T\ell\kappa}\right]^2 \mathrm{d}\kappa, \tag{13}$$

which renders a slight over-estimation. Moreover, the influence of the excitation distribution,

$$\int_0^1 \left[\frac{\sin k_T \ell \kappa}{k_T \ell \kappa}\right]^2 \mathrm{d}\kappa = \frac{1}{k_T \ell}\left(\frac{\cos(2k_T\ell) - 1}{2k_T\ell} + \mathrm{Si}(2k_T\ell)\right),$$

can also be approximated. For Helmholtz numbers below unity, the cosine can be expanded and the sine integral can be linearized to give,

$$\mathrm{Re}[\overline{Y^{C\infty}_{\nu F,\, s}}] \approx (2/\pi) k_T \ell \sqrt{(1 - \nu/2}; \quad k_T \ell \leqslant \pi/4, \tag{14}$$

whereas in the case of Helmholtz numbers larger than unity, retaining the assumption that the integrand can be treated as a constant, the sine integral term can be set to $\pi/2$ in an overall sense and the cosine term neglected implying that the slope of the real part is reduced as,

$$\mathrm{Re}[\overline{Y^{C\infty}_{\nu F,\, s}}] \approx \sqrt{(1 - \nu/2}; \qquad k_T \ell \geqslant \pi/4 \tag{15}$$

In an absolute sense, the real part of the force mobility therefore increases with frequency in the region below a unity Helmholtz number to become practically frequency independent there above.

In contrast, the real part of the integrand in equation (11) is not so amenable to approximate analysis or computations. It is clear, however, that the main contribution to the integral stems from the part above the pole since the positive and negative peaks tend to cancel. The lower limit of integration, accordingly, can be elevated somewhat from unity. Although, for small enough Helmholtz numbers, the factor of the integrand relating to the excitation can be set to unity, this is not applicable since the integral becomes divergent. Accordingly, the linear theory response to a true point force excitation will be physically singular. It is therefore necessary to retain the distributed excitation in assessing the imaginary part of the mobility.

For the major part of the integration range, the kernel is essentially inversely proportional to κ such that the imaginary part of the mobility can be approximated as

$$\mathrm{Im}[\overline{Y^{\infty}_{\nu F,\, s}}] \approx \frac{2}{\pi}\frac{k_T \ell}{1 + \nu}\int_M^{\infty} \left[\frac{\sin k_T \ell \kappa}{k_T \ell \kappa}\right]^2 \quad \frac{\mathrm{d}\kappa}{\kappa}, \tag{16}$$

where M is a number slightly larger than κ_R. For small Helmholtz numbers and limited κ, it is observed that the integral will have a predominantly logarithmic behaviour except for the range close to the lower limit. As κ grows, the integrand overall becomes inversely proportional to the third power of κ. Following this reasoning, two principle dependencies can be introduced,

$$\mathrm{Im}[\overline{Y^{\infty}_{\nu F,\, s}}] \propto \frac{2}{\pi}\frac{k_T \ell}{1 + \nu}\left\{\begin{array}{ll} \ln[\alpha_1/\alpha_2 k_T \ell]; & k_T \ell \leqslant \xi, \\ \alpha_3/\alpha_4 (k_T \ell)^2; & k_T \geqslant \xi. \end{array}\right\} \tag{17a, b}$$

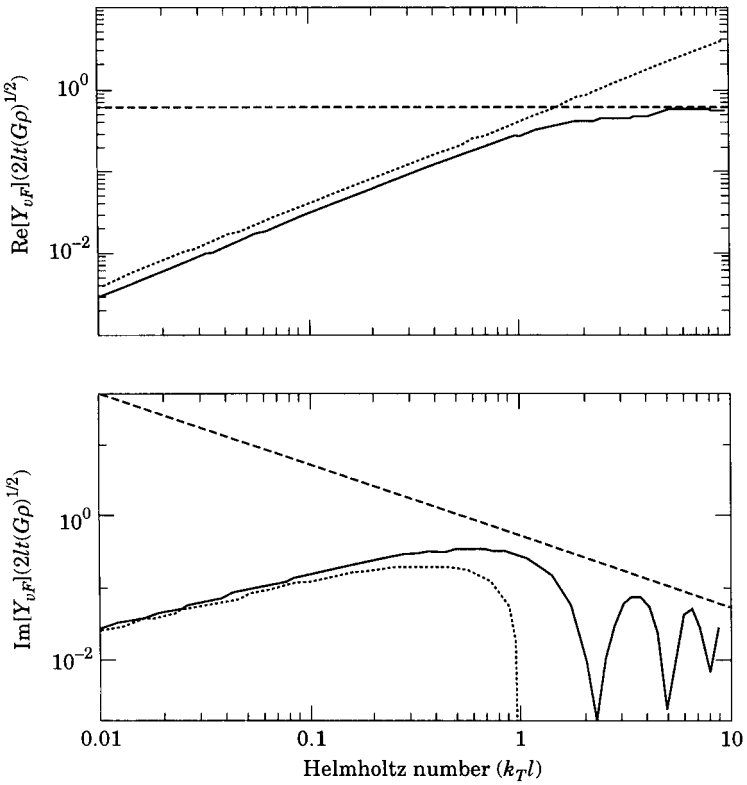

Figure 3 Normalized real (top) and imaginary (bottom) parts of edge mobility. (—) Numerical evaluation Approximations for small (· · · ·) and large (- - -) Helmholtz numbers.

The constants α_1–α_4 can be chosen such that an adequate crossover is established for a Helmholtz number of ξ.

To gain additional confidence in the functional dependencies introduced above it is observed that the integral in equation (16) has a series type of solution whereby,

$$\mathrm{Im}[\overline{Y^{\infty}_{\nu F,\,s}}] \approx \frac{2}{\pi}\frac{k_T\ell}{1+\nu}\left\{-\frac{\sin k_T\ell M}{k_T\ell M}\left(\frac{\sin k_T\ell M}{2k_T\ell M}+\cos k_T\ell M\right)-\mathrm{Ci}(2k_T\ell M)\right\}.$$

Again, for small Helmholtz numbers the trigonometric terms can be expanded while the cosine integral can be substituted by,

$$\mathrm{Ci}(\alpha z) \rightarrow -(\alpha z)^2/4+\ln(\alpha z)+\gamma_E,$$

such that,

$$\mathrm{Im}[\overline{Y^{\infty}_{\nu F,\,s}}] \propto -(2k_T\ell/[\pi(1+\nu)])\ln(2k_T\ell M).$$

In the region above, one finds that the dominant term yields,

$$\mathrm{Im}[\overline{Y^{\infty}_{\nu F,\,s}}] \propto 2/\pi(1+\nu)k_T\ell M.$$

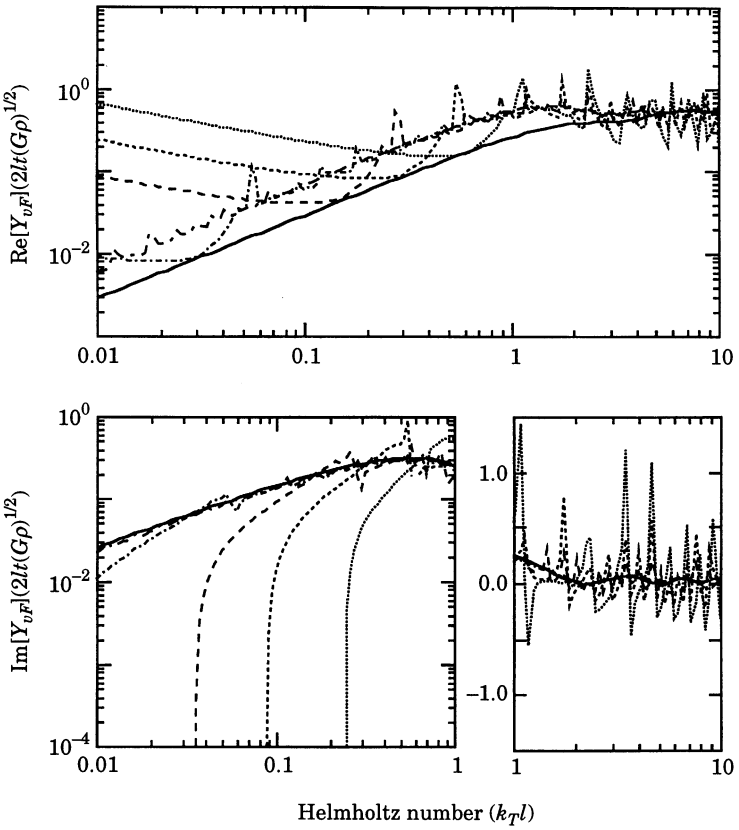

Figure 4. Normalized real (top) and imaginary (bottom) parts of mobility of edge-excited semi-infinite plate ---- and deep beams; ····· $H/\ell = 5$; - - -, $H/\ell = 10$; ——, $H/l = 20$; - · - · - $H/l = 100$, and – · –, $H/\ell = 1000$.

Accordingly, the imaginary part of the force mobility will have a logarithmic weighting in the region below unity to decrease linearly in the upper with oscillations around zero. This suggests that although the imaginary part is positive for small Helmholtz numbers, the shear–tensional nearfield cannot be regarded as a pure local deformation, cf. reference [1].

In order to test this indication, the transfer mobility can be considered which in the case of very deep beams, tends to,

$$\overline{Y^{C\infty}_{\nu F,\,s}}(x) \to -\frac{\mathrm{i}}{\pi} k_T \ell \int_0^\infty \left[\frac{\sin k_T \ell \kappa}{k_T \ell \kappa}\right] \frac{\sqrt{\kappa^2[(1-\nu)/2]}\cos(k_T x \kappa)\,\mathrm{d}\kappa}{[(2\kappa^2-1)^2 - 4\kappa^2\sqrt{\kappa^2-[(1-\nu)/2]}\sqrt{\kappa^2-1}]} \tag{18}$$

This demonstrates that, besides the propagation dependence, there is no explicit dependence on distance. Upon applying the reasoning introduced above, it can be shown that for small Helmholtz numbers, the integral, again, results in a logarithmic dependence,

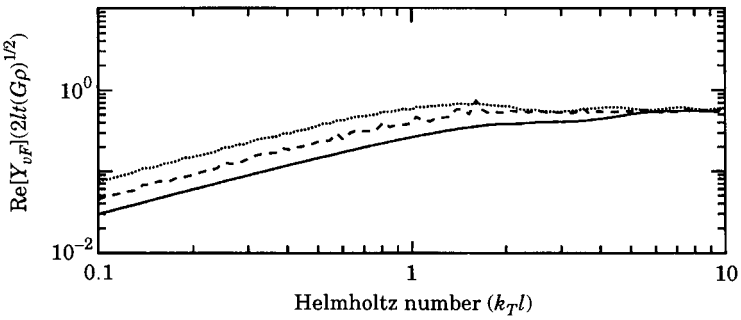

Figure 5. Normalized real part of mobility of edge-excited semi-infinite plate —— and deep beam with $H/\ell = 1000$; $\eta = 10^{-3}$ ····· and $\eta = 10^{-6}$ - - -.

$$\mathrm{Im}[\overline{Y^{C\infty}_{\nu F,\,s}}(x)] \propto -[2k_T\ell/(\pi(1+\nu))]\ln(k_T x M), \tag{19}$$

which differs from the characteristic $1/x$ dependence of a pure local deformation [7].

In Figure 3 are compared the numerically evaluated, normalized real and imaginary parts of the edge mobility with the corresponding approximations from equations (13) and preponderant functional dependencies from equations (17) respectively. It is observed from Figure 3 that the real part approximation for small Helmholtz numbers overestimates the numerically evaluated mobility. This is due to the approximation with the integrand set constant, a value which is about 25% too high in comparison with that obtained numerically. In the same region, the approximation for the imaginary part satisfactory presents the principle behaviour. For large Helmholtz numbers, the real part of the mobility approaches the asymptotic behaviour in a weakly oscillating manner while the

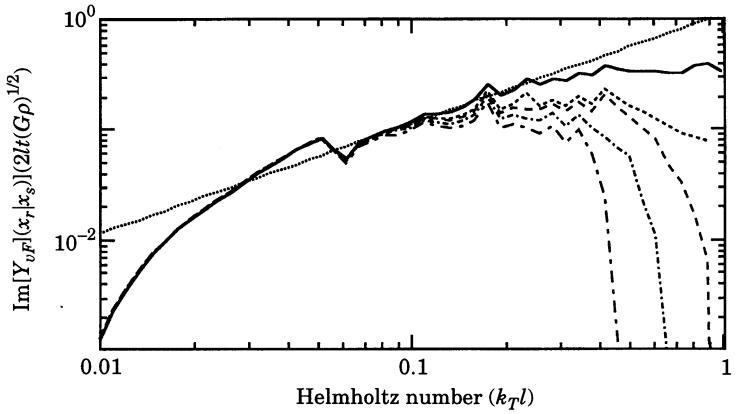

Figure 6. Normalized imaginary part of transfer mobility for a deep beam with $H/\ell = 100$; —, $x/\ell = 0$, - - - $x/\ell = 1$; —— $x/\ell = 1{\cdot}1$; - · - · -, $x/\ell = 1{\cdot}3$; — · — $x/\ell = 1{\cdot}5$ and ·····, slope of a stiffness governed mobility.

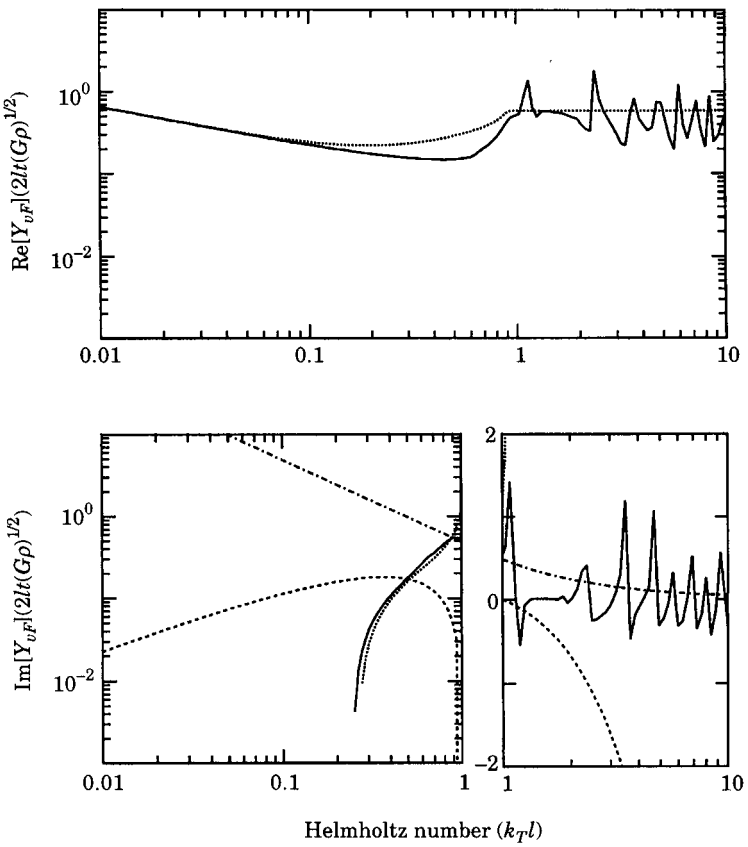

Figure 7. Normalized real (top) and imaginary (bottom) parts of deep beam mobility, $H/\ell = 5$. —— Numerical evaluation Approximations according to ····· equations (11), ---- (14) and (14a); -·-·-, (15) and (17b).

imaginary part exhibits pronounced peaks and troughs relating to the distributed excitation. For the latter part therefore, the derived base function for the upper range can be brought to establish the peak envelope.

Upon comparing the edge-excited plate mobility with that of the beam for various depth to indenter lengths, see Figure 4, it is seen that while the edge mobility of the semi-infinite plate consistently constitutes the lower limit regarding the real part for small Helmholtz numbers, it is the upper limit for the imaginary part. In the "stiffness governed" region, moreover, the slope of the imaginary part of the beam mobility changes markedly as the depth to indenter length ratio changes. For the upper range of Helmholtz numbers, the real part of the beam mobility tends to that of the edge-excited plate irrespective of depth whereas a pronounced wave guide behaviour dominates the imaginary part for depth to indenter length ratios below 100.

The observation that the real part of the beam mobility generally has a higher value than the semi-infinite plate in an intermediate region can be explained by the dissipative losses present for the former structure while the plate is treated as non-dissipative. In Figure 5 is shown the real part of the beam mobility in the

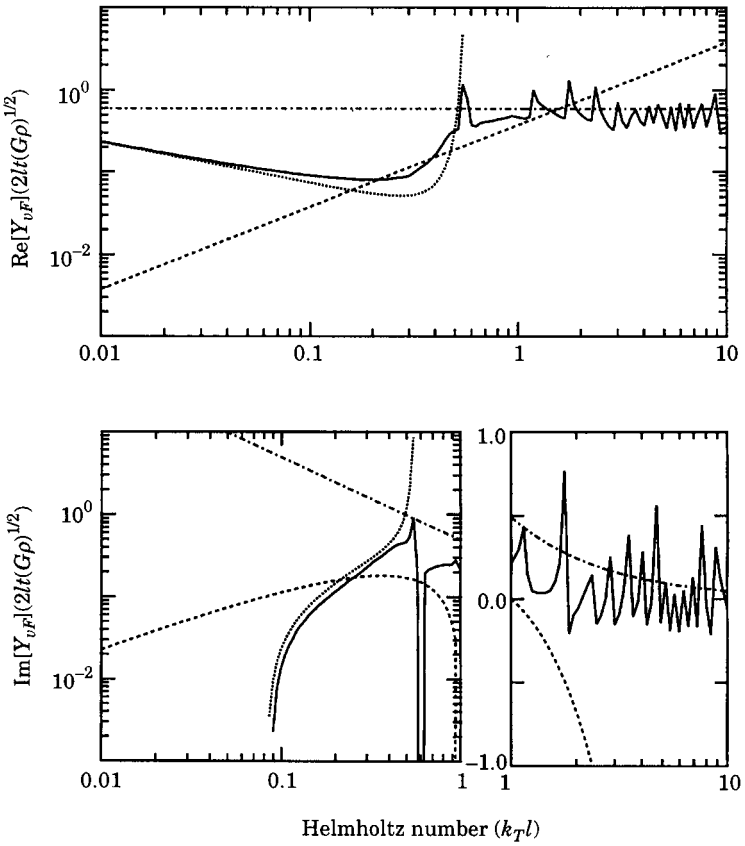

Figure 8. Normalized real (top) and imaginary (bottom) parts of deep beam mobility, $H/\ell = 10$. —— Numerical evaluation Approximations according to equations ·····, (11); ---, (14) and (17a); -·-·-, (15) and (17b).

extreme case of $H/\ell = 1000$ for two different values of the loss factor. As the dissipative losses are reduced a reduction of the real part is manifested for Helmholtz numbers smaller than unity. For the upper range, however, the results are, as expected, unaffected. Physically, this originates from the so-called Lamb waves, cf. references [6, 8], present in the finite depth case, which, owing to the losses, also establish small but numerous propagating wave components. It should be pointed out that in the numerical evaluation of the beam mobility, a loss factor of 10^{-3} was assigned as the reference value. Therefore, in order to account for the surface wave contributions, the characteristic mobility of shear waves can be employed in this range.

The transfer mobilities to positions at the end of and just outside the indenter are shown in Figure 6. From this comparison a small variation with distance is evident in the region where the mobility follows that of a pure stiffness. This variation, however, is not typical for a local deformation where the mobility decreases rapidly outside the excited area [7]. Moreover, it is observed that the variation increases with Helmholtz number, another aspect which is not

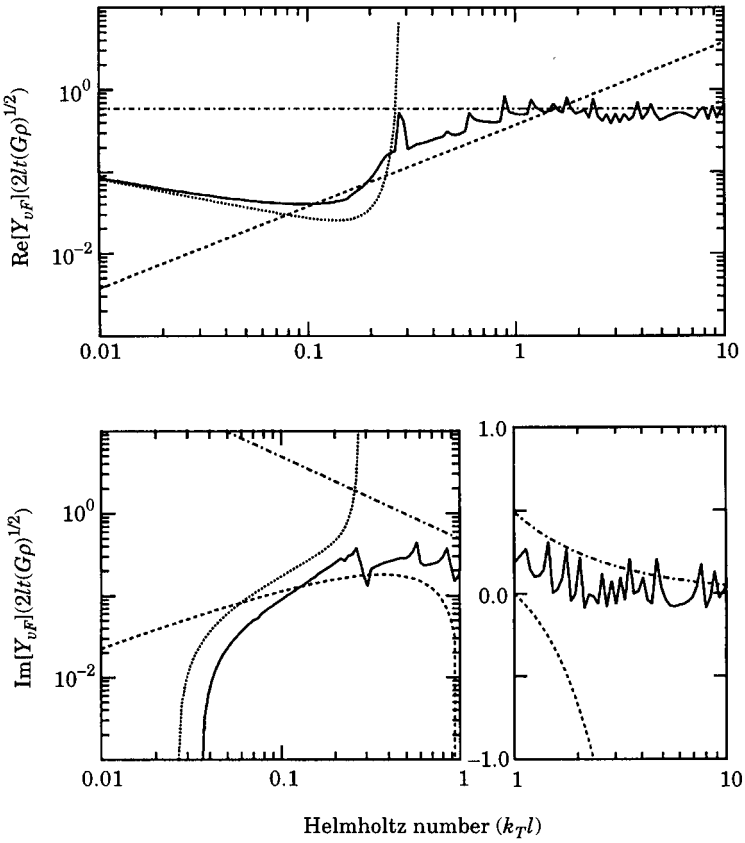

Figure 9. Normalized real (top) and imaginary (bottom) parts of deep beam mobility, $H/\ell = 20$. —— Numerically evaluation Approximations according to equations ·····, (11); ---, (14) and (17a) -·-·-, (15) and (17b).

typical for a mobility controlled by local deformation but rather allied with propagating waves.

3. COMPARISON OF APPROXIMATIONS AND NUMERICAL RESULTS

In Figures 7–11, the trends of the closed form approximations established in the preceding section are compared with the numerically evaluated results. For the real part it is clear that there are two ingredients involved below the fundamental dilatational resonance. The lower asymptote, as expected, is that of a slender beam. From the anti-resonant region and beyond the dilatational resonance, the higher order waves contribute, supplemented by energy propagation due to the evanescent waves. In the region above Helmholtz number equal to unity, the beam behaves essentially as a rod of cross-sectional dimensions equal to the width of the beam and the length of the indenter cf. reference [1]. With respect to the imaginary part, a similar transition is observed with the slender beam behaviour governing the small Helmholtz number range

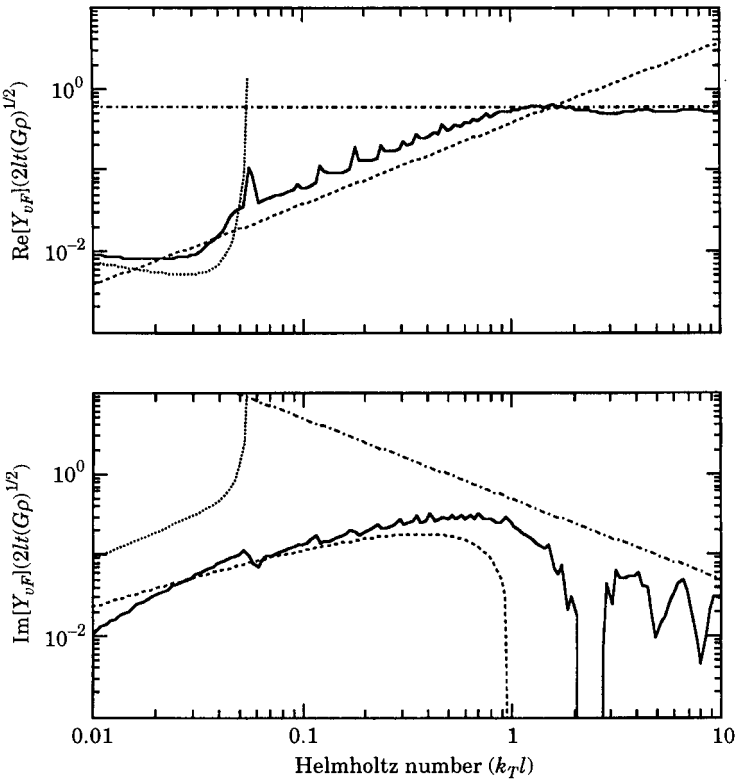

Figure 10. Normalized real (top) and imaginary (bottom) parts of deep beam mobility, $H\ell = 100$. —— Numerical evaluation Approximations according to ·····, equations (11); ---, (14) and(17a); -·-·-, (15b) and (17b).

up to the anti-resonance. There above, a distinction must be made between moderately deep and deep beams respectively. In the former case the waveguide effects are pronounced and sharp peaks and troughs relating to the onset of higher order travelling waves dominate the pattern. For the latter case however, such a waveguide behaviour is shadowed by the influence of the distributed excitation establishing a smoother pattern with peaks and troughs largely controlled by the excitation wavenumber spectrum. Also the overall decrease and asymptotic vanishing of the imaginary part become more clear for deep beams.

From the comparison with the closed form approximations derived, it is evident that the real part can be satisfactorily described in the lower and upper regions by the respective asymptotes. For the intermediate range, however, a combination of the approximations appears to be required to take into account the dilatational resonance as well as the energy propagation by higher order waves. With respect to the imaginary part the distinction between moderately deep and deep beams must be observed. For $H/\ell \leqslant 10$, the slender beam behaviour satisfactorily describes the low Helmholtz number range while the infinitely deep beam envelope only in an overall sense depicts the behaviour in the upper range. At the resonance, the contribution from the quasi-longitudinal

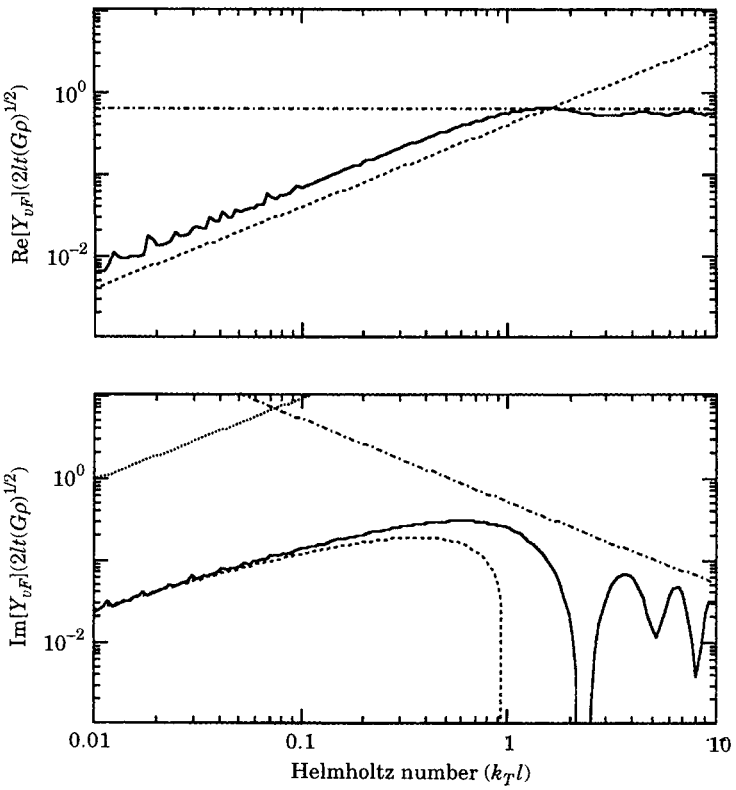

Figure 11. Normalized real (top) and imaginary (bottom) parts of deep beam mobility, $H/\ell = 1000$. —— Numerical evaluation Approximations according to ·····, equations (11); - - - (14) and (17a) -·-·-, (15) and (17b).

wave has to be included. For larger ratios H/ℓ, the intermediate range of Helmholtz numbers is increasingly dominated by the high order travelling and evanescent waves and the influence of the dilatational resonance is markedly reduced. This means that the logarithmically weighted stiffness approximation applies.

In Figures 12 and 13, two previously reported approximations for the imaginary part of the force mobility are compared with the numerical results for two different beam configurations. It is seen that while the approximation developed by Heckl [4], irrespective of beam height to indenter length ratio, gives a satisfactory description of the imaginary part for small Helmholtz numbers, the approximation proposed by Ljunggren [5] renders an over-estimate.

4. ESTIMATION PROCEDURE

Based on the preceeding theoretical and numerical analysis, an estimation procedure for the edge-excited deep beam can be developed. For the real part, the region of small Helmholtz numbers is essentially controlled by the beam characteristics up to the fundamental dilatational resonance. From the preceding

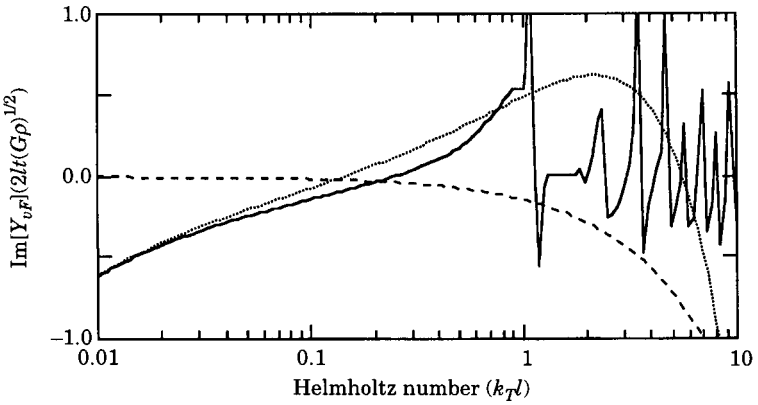

Figure 12. Normalized imaginary part of deep beam mobility, $H/\ell = 5$: ————, numerically evaluated; · · · · · ·, approximations according to Heckl [4] and - - -, Ljunggren [5].

anti-resonant region where the minimum is set by the real part of the edge-excited semi-infinite plate, the mobility rises to the resonance. Above the resonance, the behaviour is in general governed by the energy propagated by quasi-longitudinal waves in an equivalent rod but the depth of the beam controls the transition. For small ratios of depth to indenter length, the real part settles at the characteristic rod mobility almost immediately above the dilatational resonance. As the depth to indenter ratio increases, all in-plane waves carry energy and an intermediate region is established in which the real part overall increases linearly.

With respect to the imaginary part a distinction must be made between moderately deep and deep beams since in the former case, as for the real part, the dilatation resonance markedly affects the dynamics. In the case of deep beams a procedure for the imaginary part, in the range above that of beam

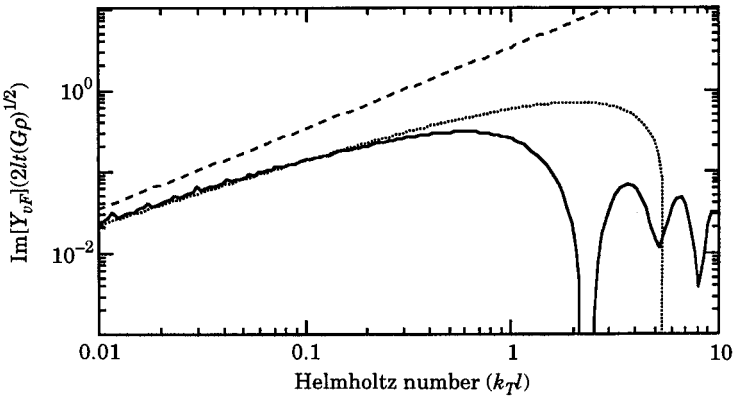

Figure 13. Normalized imaginary part of deep beam mobility, $H/\ell = 1000$: —, numerically evaluated; · · · · · ·, approximations according to Heckl [4] and - - -, Ljunggren [5].

TABLE 1

Estimation procedure for the real part of the force mobility of deep beams

$\mathrm{Re}[Y^{C\infty}_{\nu F,\,s}]$	$\dfrac{\omega}{4Bk_B^3}+\sqrt{\dfrac{(1-\nu)}{2}}\dfrac{k_t\ell}{\pi\ell t\sqrt{G\rho}}\left(1+\dfrac{(9\pi\nu^2/2)k_TH}{(72(1+\nu)-3(2-\nu^2)(k_TH)^2+[(1-\nu)/8](k_TH)^4)}\right);$ $\quad k_TH\leqslant\sqrt{6(1+\nu)}$
	$\mathrm{Min}\begin{cases}\dfrac{\omega}{4B_B^3}+\sqrt{\dfrac{(1-\nu)}{2}}\dfrac{k_T\ell}{\pi\ell t\sqrt{G\rho}}\left(1+\dfrac{(9\pi\nu^2/2)k_TH}{(72(1+\nu)-3(2-\nu^2)(k_TH)^2+[(1-\nu)/8](k_TH)^4)}\right); & k_TH\geqslant\sqrt{6(1+\nu)}\\ \dfrac{k_T\ell}{\pi\ell t\sqrt{G\rho}} & \\ \dfrac{1}{2\ell t\sqrt{G\rho}}\sqrt{\dfrac{(1-\nu)}{2}} & \end{cases}$

TABLE 2

Estimation procedure for imaginary part of force mobility of deep beams

$\mathrm{Im}[Y^{C\infty}_{vF,s}]$ $H/\ell \leqslant 10$	$-\dfrac{\omega}{4Bk_B^3}+\dfrac{k_T H}{2\ell t\sqrt{G\rho}}\left\{\dfrac{(1-\nu)}{8}+\left(\dfrac{9\nu^2}{(72(1+\nu)-3(2-\nu^2)(k_T H)^2+[(1-\nu)/8](k_T H)^4)}\right)\right\}; \quad k_T H \leqslant 2\sqrt{6(1+\nu)}$ $\dfrac{1}{\pi\ell t\sqrt{G\rho}}\dfrac{k_T\ell}{(1+\nu)}\dfrac{\ln[2(1+\nu)]\sin^2(1+\nu)}{(1+\nu)^2(k_T\ell)^2}; \quad k_T h > 2\sqrt{6(1+\nu)}$
$\mathrm{Im}[Y^{C\infty}_{vF,s}]$ $H/\ell \geqslant 10$	$k_T\ell \leqslant \pi/(1+\nu)$ $-\dfrac{\omega}{4Bk_b^3}+\dfrac{1}{\pi\ell t\sqrt{G\rho}}\dfrac{k_T\ell}{(1+\nu)}$ $\times \ln\left[\dfrac{2(1+\nu)}{k_T\ell}\right]\left(\dfrac{\sin(1+\nu)k_T\ell}{(1+\nu)k_T\ell}\right)^2$
	$k_T\ell \leqslant \pi/(1+\nu)$ $\dfrac{\ln[2(1+\nu)]\left(\dfrac{\sin(1+\nu)k_T\ell}{(1+\nu)k_T\ell}\right)^2}{\pi\ell t(1+\nu)k_T\ell\sqrt{G\rho}}$

behaviour, is proposed to follow,

$$\mathrm{Im}[\overline{Y^{\infty}_{\nu F,\,s}}] \approx \frac{2}{\pi}\frac{k_T\ell}{(1+\nu)}\left(\frac{\sin(1+\nu)k_T\ell}{(1+\nu)k_T\ell}\right)^2 \left\{ \begin{array}{ll} \ln\left[\dfrac{2(1+\nu)}{k_T\ell}\right]; & k_T\ell \leqslant \dfrac{\pi}{1+\nu} \\ \dfrac{\ln[2(1+\nu)]}{(k_T)^2}; & k_T\ell \geqslant \dfrac{\pi}{1+\nu} \end{array} \right\}. \quad (20)$$

The choice for relating the constants to the material properties is based upon the results of parameter studies but it must be emphasized that even though the functional dependencies are theoretically qualified, the fitted constants are only numerically underpinned and not explicitly proven.

Upon compiling the various expressions for the different regions and different ratios of beam depth to indenter length, the estimation procedure proposed is summarized in Tables 1 and 2. The estimated mobilities for two radically different beam configurations are exemplified in Figures 14 and 15.

For both beam configurations, it is seen that overall a conservative estimate is established with respect to the real part. Since only a single higher order mode is included to establish the dilatational resonance, an under-estimate would result in the anti-resonant region from beam behaviour only. Moreover, the estimated response at the dilatational resonance would be incorrect. Unfortunately, the

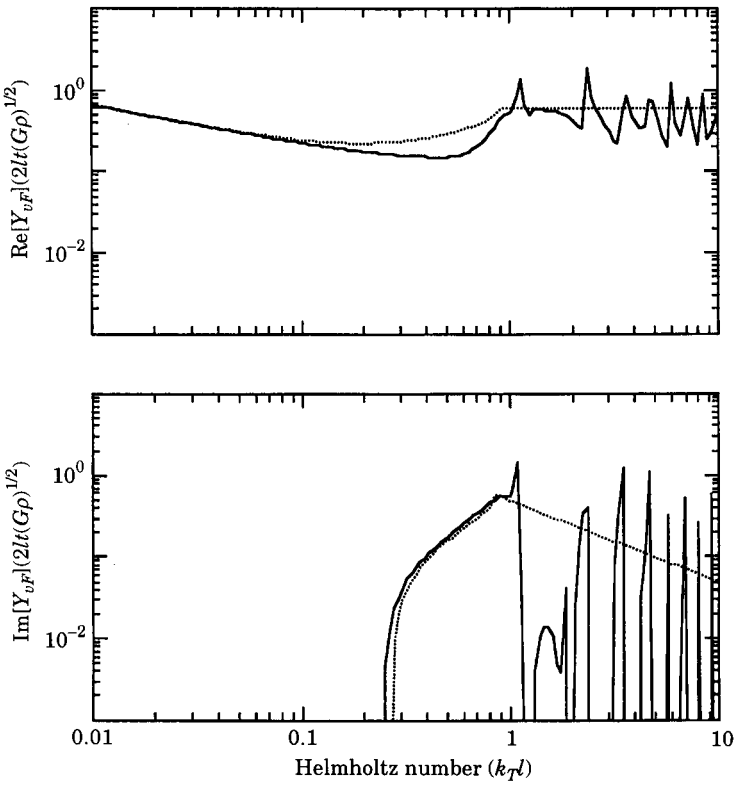

Figure 14. Comparison of estimated ····· and numerically evaluated –––– force mobility; $H/\ell = 5$.

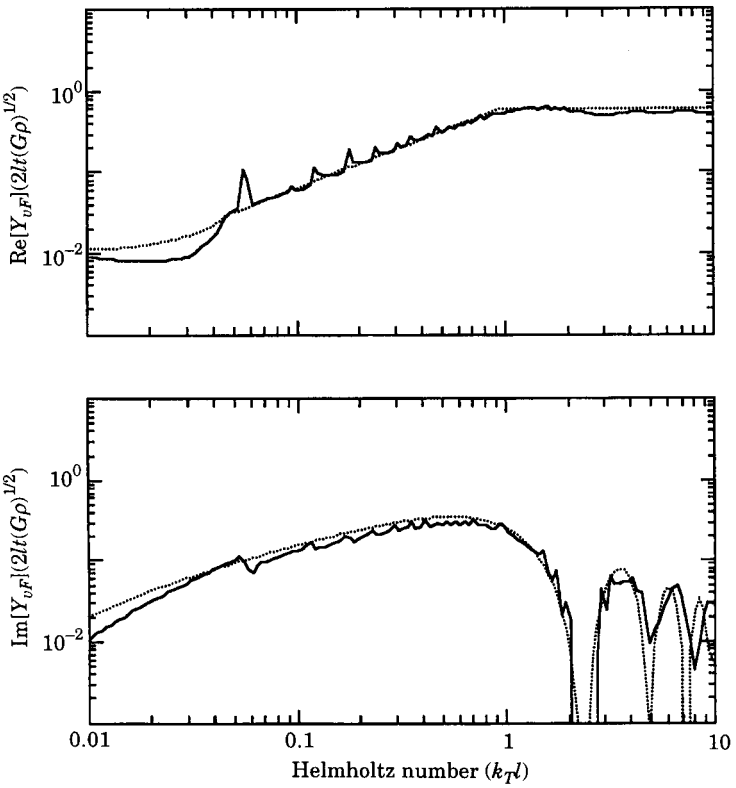

Figure 15. Comparison of estimated (· · · · ·) and numerically evaluated (– – – –) force mobility; $H/\ell = 100$.

fact that the shear–tensional nearfield converts part of the evanescent waves into propagating ones means that an estimate for the peak value becomes unwieldy. To circumvent these deficiencies, it is proposed that a summation of the contributions from higher order modes of vibration as given by the edge-excited, semi-infinite plate and that from the single dilatational mode, approximately accounts for the energy transmission in the transition region. For deep beams, the discrepancy following from the non-dissipative model for the edge-excited semi-infinite plate is taken into account by relating the estimation to shear waves.

Regarding the imaginary part for moderately deep beams, the estimation procedure compares satisfactorily with calculated results up to the dilatational resonance. Again, the complication at the resonance stemming from the intricate wave field is circumvented. In the upper region the procedure captures the overall trend but ignores the waveguide effects.

Overall the estimation procedure performs satisfactorily for the imaginary part and deep beams. Discrepancies are primarily found towards the lower and upper ends of the interval considered. The asymptotic beam behaviour, however, is guaranteed for Helmholtz numbers tending to zero. At the upper end of the interval it is seen that the modulation due to the distributed excitation only is captured approximately.

5. CONCLUDING REMARKS

This study, devoted to two-dimensional wave-guides, clearly highlights the intricate interplay between propagating and evanescent waves for moderately deep and deep beams, making the development of physically correct, yet manageable estimation procedures more challenging than in the case of thick plates.

It can be concluded that for deep beams, ideal point excitation realizes an infinite, linear theory response. The dynamic characteristics of this structural system therefore imply a distributed excitation with its features primarily manifested in the region of Helmholtz numbers larger than π. It is further found that, as for plates, the shear–tensional nearfield plays a significant role for the dynamic characteristics of deep beams but from the frequency where the cross-sectional, in-plane motion opposes the slender beam bending behaviour (rigid beam lamina). Above this transition, from essentially mass- to stiffness-controlled behaviour in the force mobility case, the analysis shows that Lamb waves contribute to the propagation of energy when dissipation in physically realistic materials is taken into account. This phenomenon hence constitutes a clear distinction between deep and infinitely deep beams since the Lamb waves are annulled for the latter configuration. It can thus be concluded that the real part of the force mobility is larger in the finite case than in the infinite in this range up to the point where the length of the excitation area equals half the wavelength of the shear wave. For larger Helmholtz numbers, the active, finite depth characteristics approach those of the infinite case which can be interpreted as those of an axially excited rod of cross-section equal to that of the excitation area. This has a correspondence in the case of fluid-borne sound where the lobes from a radiator becomes highly directive.

For the reactive part of the dynamic characteristics, the infinitely deep beam furnishes a valid model in the intermediate range whereas the waveguide effects dominate the characteristics for large Helmholtz numbers and finite depths which are not easily captured in closed form. The envelope to the dynamic characteristics of infinitely deep beams in the upper range, however, establishes the overall trend. Based on the edge-excited, semi-infinite plate model, a logarithmically weighted, stiffness controlled response is inferred above the dilatational resonance. Owing to the logarithmic weighting therefore, it is strictly not correct to regard the shear–tensional nearfield effects as pure local deformation.

ACKNOWLEDGMENT

Financial support has been received from the TNO Defence Research Organisation.

REFERENCES

1. B. A. T. Petersson and M. Heckl 1996 *Journal of Sound and Vibration* **196**, 295–321. Concentrated excitation of structures.

2. H. LAMB 1904 *Philosophical Transactions of Royal Society* **A203**, 1–42. On the propagation of tremors over the surface of an elastic solid.
3. G. F. MILLER and H. PURSEY 1954 *Proceedings of Royal Society* **A223**, 521–541. The field and radiation impedance of mechanical radiators on the free surface of a semi-infinite isotropic solid.
4. M. HECKL 1981 *Acustica* **49**, 183–191. Körperschallübertragung bei homogenen Platten beliebiger Dicke.
5. S. LJUNGGREN 1989 *Journal of The Acoustical Society of America* **86**, 1419–1431. Line mobilities of infinite plates.
6. B. A. AULD 1973 *Acoustic Fields and Waves in Solids* New York: Wiley-Interscience, **II**, Chapter 10.
7. B. PETERSSON, 1982 *Journal of Sound and Vibration* **91**, 219–238. An approximation for the point mobility at the intersection of two perpendicular plates.
8. K. TAMM and O. WEIS 1959 *Acustica* **9**, 275–288. Untersuchungen über periodische Wellen, exponentielle und komplexe Nahfelder im begrenzten Festkörper.

APPENDIX I: EDGE-EXCITED, SEMI-INFINITE PLATE.

Allowing the beam depth to be infinite there are no reflected waves and the potential and stream functions take the forms,

$$\Phi(x, y) = \Phi_+ e^{-iq_L y}\, e^{ikx}, \qquad \Psi(x, y) = \Psi_+\, e^{-iq_T y}\, e^{ikx}. \tag{AI.1a, b}$$

With the particle velocity and the pertinent stresses as given in reference [1], i.e.,

$$v_y = \partial\Phi/\partial y - \partial\Psi/\partial x, \tag{AI.2}$$

and

$$\sigma_y = \frac{2G}{i\omega(1-\nu)}\left[\frac{\partial^2\Phi}{\partial y^2} + \nu\frac{\partial^2\Phi}{\partial x^2} - (1-\nu)\frac{\partial^2\Psi}{\partial x\partial y}\right],$$

$$\tau_{xy} = \frac{2G}{i\omega}\left[\frac{\partial^2\Phi}{\partial x\partial y} + \frac{1}{2}\left(\frac{\partial^2\Psi}{\partial y^2} - \frac{\partial^2\Psi}{\partial x^2}\right)\right]$$

respectively and the conditions at the boundary $y = 0$,

$$\sigma_y = \begin{cases} \hat{\sigma}\, e^{ikx}; & |x| \leqslant \ell \\ 0 \quad ; & |x| > 0 \end{cases} \quad \text{and} \quad \tau_{xy} \equiv 0. \tag{AI.3a, b}$$

The relation between the unknown coefficients is found to be given by

$$\Psi_+ = -\hat{\sigma}\frac{i\omega}{G} 2q_L k/[(2k^2 - k_T^2)^2 + 4q_L q_T k^2] \tag{AI.4}$$

and

$$\Phi_+ = \hat{\sigma}\frac{i\omega}{G}(2k^2 - k_T^2)/[(2k^2 - k_T^2)^2 + 4q_L q_T k^2]. \tag{AI.5}$$

This means that the particle velocity becomes,

$$v_y = -\hat{\sigma}\frac{\omega}{G}k_T^2\{(q_L/[2k^2 - k_T^2)^2 + 4q_Lq_Tk^2]\}\ \mathrm{e}^{-\mathrm{i}q_Ly}\ \mathrm{e}^{\mathrm{i}kx}. \tag{AI.6}$$

Assuming a soft indenter, the stress wavenumber spectrum is obtained as

$$\hat{\sigma}(k, z) = \frac{F}{2lt}\int_{-\ell}^{\ell} \mathrm{e}^{\mathrm{i}kx}\,\mathrm{d}x = \frac{F}{t}\frac{\sin k\ell}{k\ell} \tag{AI.7}$$

and applying the inverse transform, the mobility is found to be given by,

$$Y_{vF}^{\infty} = -\frac{\omega}{2\pi Gt}k_T^2\int_{-\infty}^{\infty}\left[\frac{\sin k\ell}{k\ell}\right]^2\frac{q_L\ \mathrm{e}^{\mathrm{i}q_Ly}\,\mathrm{d}k}{[(2k^2 - k_T^2)^2 + 4q_Lq_Tk^2]}.$$

By specializing on the "point" mobility on a complex power basis and recognizing that the integrand is symmetric yields the normalized result,

$$\overline{Y_{vF}^{\infty}} = -\frac{2k_T\ell}{\pi}k_0^2\int_0^{\infty}\left[\frac{\sin k\ell}{k\ell}\right]^2 q_L\,\mathrm{d}k/[(2k^2 - k_T^2)^2 + 4q_Lq_Tk^2]. \tag{AI.8}$$

Owing to the branch points, three regions of integration have to be considered:

$$S = k_T^2\int_0^{\infty}\left[\frac{\sin k\ell}{k\ell}\right]^2\frac{q_L\,\mathrm{d}k}{[(2k^2 - k_T^2)^2 + 4q_Lq_Tk^2]}$$

$$= \left\{\begin{array}{ll} \displaystyle\int_0^{\beta}\left[\frac{\sin k_T\ell\kappa}{k_T\ell\kappa}\right]^2\frac{-\sqrt{\beta^2-\kappa^2}\,\mathrm{d}\kappa}{[(2\kappa^2-1)^2 + 4\kappa^2\sqrt{\beta^2-\kappa^2}\sqrt{1-\kappa^2}]}; & \kappa^2 \leqslant \beta^2, \\ \displaystyle\int_{\beta}^{1}\left[\frac{\sin k_T\ell\kappa}{k_T\ell\kappa}\right]^2\frac{\mathrm{i}\sqrt{\kappa^2-\beta^2}\,\mathrm{d}\kappa}{[(2\kappa^2-1)^2 - \mathrm{i}4\kappa^2\sqrt{\kappa^2-\beta^2}\sqrt{1-\kappa^2}]}; & \beta^2 \leqslant \kappa^2 \leqslant 1, \\ \displaystyle\int_1^{\infty}\left[\frac{\sin k_T\ell\kappa}{k_T\ell\kappa}\right]^2\frac{\mathrm{i}\sqrt{\kappa^2-\beta^2}\,\mathrm{d}\kappa}{[(2\kappa^2-1)^2 - 4\kappa^2\sqrt{\kappa^2-\beta^2}\sqrt{\kappa^2-1}]}; & 1 \leqslant \kappa^2, \end{array}\right\} \tag{AI.9}$$

where $\beta^2 = (1-\nu)/2$.

APPENDIX II: SYMBOLS AND NOTATION

B	flexural stiffness
E	Young's modulus
F	force
G	shear modulus
H	beam height
I	integral
M	integration limit
N	denominator

R residue
S area
Y mobility
g integration factor
h half the beam height
i imaginary unit
k wavenumber
ℓ half the length of indenter
m'' mass per unit area
q wavenumber radical
t width of beam
v translational velocity
x, y, z Cartesian co-ordinates
Φ potential function
Ψ stream function
Λ norm
α factor
β auxiliary variable
ε small number
γ_E Euler's constant
λ wavelength
κ normalized wavenumber
ξ number
ξ, η, ζ Cartesian co-ordinates
η loss factor
ω angular frequency
ρ density
σ normal stress
τ shear stress
ν Poisson's ratio

indices:

B flexural
C continuum
F force
L longitudinal
R Rayleigh wave
T transverse
n order
s soft indenter, source
v lateral translational velocity

notation:

$\bar{\ }$ normalized quantity